AD-A125 763 MATERIALS RESEARCH FOR ADVANCED INERTIAL INSTRUMENTATION TASK 1 DIMENSION..(U) CHARLES STARK DRAPER LAB INC CAMBRIDGE MA K KUMAR ET AL. DEC 82 1/1

UNCLASSIFIED R-1612 N00014-77-C-0388 F/G 17/7 NL

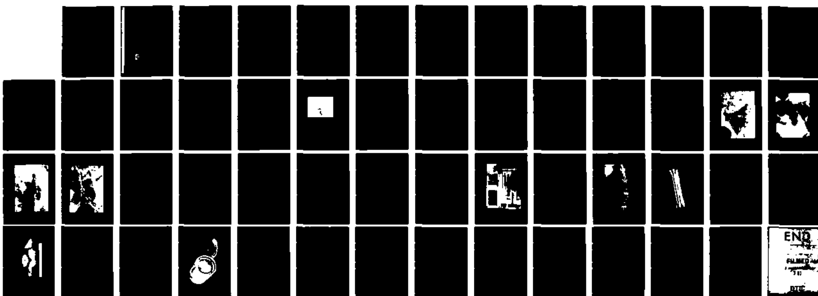

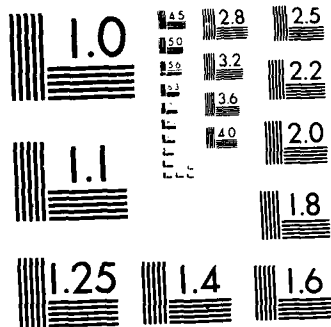

MICROCOPY RESOLUTION TEST CHART
NATIONAL BUREAU OF STANDARDS-1963-A

AD A 125763

CSDL - R - 1612

MATERIALS RESEARCH FOR ADVANCED INERTIAL INSTRUMENTATION TASK 1: DIMENSIONAL STABILITY OF GYRO SCOPE STRUCTURAL MATERIALS

DECEMBER 1982

TECHNICAL REPORT NO. 5

FOR THE PERIOD

1 OCTOBER 1981 - 30 SEPTEMBER 1982

K. Kumar, D. Cardarelli, F. Petri

Prepared for the Office of Naval Research,
Department of the Navy, under Contract N00014-77-C-0388

Approved for Public Release; distribution unlimited.

Permission is granted to the U.S. Goverment
to reproduce this report in whole or in part.

DTIC

The Charles Stark Draper Laboratory, Inc.
Cambridge, Massachusetts 02139

DTIC FILE COPY

83 03 17 001

SECURITY CLASSIFICATION OF THIS PAGE *(When Data Entered)*

REPORT DOCUMENTATION PAGE		READ INSTRUCTIONS BEFORE COMPLETING FORM
1. REPORT NUMBER Technical Report No. 5	2. GOVT ACCESSION NO. AD-A125 783	3. RECIPIENT'S CATALOG NUMBER
4. TITLE *(and Subtitle)* Materials Research for Advanced Inertial Instrumentation, Task 1: Dimensional Stability of Gyroscope Structural Materials		5. TYPE OF REPORT & PERIOD COVERED Research Report 10/1/81 - 9/30/82
		6. PERFORMING ORG. REPORT NUMBER
7. AUTHOR(s) K. Kumar, D. Cardarelli, and F. Petri		8. CONTRACT OR GRANT NUMBER(s) N00014-74-C-0388
9. PERFORMING ORGANIZATION NAME AND ADDRESS The Charles Stark Draper Laboratory, Inc. 555 Technology Square Cambridge, Massachusetts 02139		10. PROGRAM ELEMENT, PROJECT, TASK AREA & WORK UNIT NUMBERS
11. CONTROLLING OFFICE NAME AND ADDRESS Office of Naval Research Department of the Navy 800 N. Quincy Street, Arlington, Virginia 20217		12. REPORT DATE December 1982
		13. NUMBER OF PAGES 55
14. MONITORING AGENCY NAME & ADDRESS *(if different from Controlling Office)* Office of Naval Research Boston Branch, Bldg. 114, Sec. D 666 Summer Street Boston, MA 02210		15. SECURITY CLASS. *(of this report)* Unclassified
		15a. DECLASSIFICATION/DOWNGRADING SCHEDULE

16. DISTRIBUTION STATEMENT *(of this Report)*

Approved for public release, distribution unlimited

17. DISTRIBUTION STATEMENT *(of the abstract entered in Block 20, if different from Report)*

18. SUPPLEMENTARY NOTES

19. KEY WORDS *(Continue on reverse side if necessary and identify by block number)*

Dimensional Stability	Microcreep
Finite Element Analysis	Micromechanical Properties
Gyroscope Materials	Microstrain Modeling
Hot Isostatically Pressed Beryllium	Microyield Strength
X-520 Beryllium	Optical and Electron Microscopy

20. ABSTRACT *(Continue on reverse side if necessary and identify by block number)*

Microstructure evaluations of HIP50 and X-520 experimentally produced grades of Be materials were continued during this reporting period. These materials were examined by transmission as well as scanning transmission electron microscopy (TEM/STEM) techniques. Gentle procedures were developed for producing appropriate samples for this purpose. Work performed during this recent study was substantially more extensive than efforts made previously and included a determination of second phase particle size, number density,

DD FORM 1473 1 JAN 73 EDITION OF 1 NOV 65 IS OBSOLETE

UNCLASSIFIED

SECURITY CLASSIFICATION OF THIS PAGE *(When Data Entered)*

elemental composition and their distribution in the material. Several notable differences were observed between the two beryllium grades and these appeared to explain the differences in the microyield strength (MYS) property behavior that was determined and reported upon in prior annual reports. It was noted that the second phase particles in both the beryllium grades, were mainly located at the grain boundaries. However, the average size of the particles in HIP50 was typically one-half of those in X-520 and their number density was also much higher. The particles were mainly composed of the oxides of Be in HIP50; however the X-520 particles almost always contained Si and Fe. These observations were in substantial agreement with SEM and X-ray results reported earlier which had suggested that the second phase particles in X-520 were composed of the Be_2SiO_4 phase. The STEM results showed however, that the particles were predominantly BeO containing possible reacted regions of the Be_2SiO_4 phase. These results indicated that to produce high MYS Be it is important to keep the Si content and consolidation temperature low. Use should be made of fine impact attritioned powder and hot isostatic pressing should be used as the densification procedure. The role of impurities, other than Si was less clearly defined. The data indicated that Fe content (to the extent present in X-520 Be) was not very significant.

A substantial amount of effort was expended on the construction of the 10^{-7} inch/inch tensile microcreep measuring facility that was designed and discussed earlier. An oven capable of controlling sample temperature within 0.02°F was constructed and tested. The load train and novel design thin film capacitive extensometer were also built. Preliminary evaluations of these components and all support electronics (that were designed and assembled) were made and determined to be quite satisfactory. Finite element modelling procedures continued to guide the development of the testing procedure. Calculations were also performed on the rate of microcreep expected at time intervals of interest on the basis of results produced at the National Bureau of Standards (NBS). These calculations indicated that on the basis of the NBS postulated behavior, microcreep in instrument grade I-400 Be was possibly not too severe a contributor to instrument behavior. However, the lack of an independent verification of these results and the lack of data at the loads which are of interest do not permit firm conclusions to be reached in this respect.

CSDL-R-1612

MATERIALS RESEARCH FOR ADVANCED INERTIAL INSTRUMENTATION

TASK 1: DIMENSIONAL STABILITY OF GYROSCOPE STRUCTURAL MATERIALS

DECEMBER 1982

TECHNICAL REPORT NO. 5

FOR THE PERIOD
1 October 1981 - 30 September 1982

Accession For
NTIS GRA&I X
Dist
A

K. Kumar, D. Cardarelli, F. Petri

Prepared for the Office of Naval Research,
Department of the Navy, under Contract N00014-77-C-0388.

Approved for Public Release; distribution unlimited.

Permission is granted to the U.S. Government
to reproduce this report in whole or in part.

Approved: M S Sapuppo
M.S. Sapuppo, Head
Component Development Department

The Charles Stark Draper Laboratory
Cambridge, Massachusetts 02139

ACKNOWLEDGEMENTS

This report was prepared by The Charles Stark Draper Laboratory, Inc. (CSDL), under Contract N00014-77-C-0388 with the Office of Naval Research (ONR), Department of the Navy.

The X-520 samples used in this study were procured from Dr. J. Smugeresky of Sandia Laboratories through the courtesy of Dr. G. London of the Naval Air Development Center. The TEM/STEM analyses were performed with Professor John B. Van der Sande of MIT serving as the consultant. This project is monitored by Dr. G. London on behalf of ONR.

Publication of this report does not constitute approval by the U.S. Navy of the findings or conclusions contained herein. It is published for the exchange and stimulation of ideas.

TABLE OF CONTENTS

Section		Page
1.	INTRODUCTION	1
2.	OBJECTIVES	3
3.	PREVIOUS WORK	5
4.	PRESENT WORK	9
4.1	Microstructure Evaluations	9
4.2	Sample Preparation for Electron Microscopic Examination	10
4.3	TEM/STEM Studies	11
4.4	X-520 Beryllium	11
4.5	HIP 50 Beryllium	18
4.6	Comparison of X-520 and HIP 50 Microstructure Data	24
4.7	Correlation of Microstructure with Microyield Behavior	25
4.8	Microcreep Modeling	27
4.9	Development of Instrumentation for Microcreep Measurement	28
	LIST OF REFERENCES	41
	DISTRIBUTION LIST	43

LIST OF FIGURES

Figure		Page
1	Annular dark-field image in stem showing second-phase particles and grains in as-received material	12
2	(X-ray) signal from large precipitate in as-received X-520 sample	17
3	As-received HIP 50. TEM micrograph	19
4	HT1-treated HIP 50. TEM micrograph	20
5	HT2-treated HIP 50. TEM micrograph	21
6	HT3-treated HIP 50. TEM micrograph	22
7	CSDL-designed/microcreep testing apparatus	29
8	Load train for microcreep measurement	31
9	Typical microcreep specimen	32
10	Capacitive extensometer plates	35
11	Capacitive film patterns	37
12	Oven for controlling specimen temperature	38
13	Microcreep test thermal chamber	39
14	Schematic diagram showing capacitive signal detection of microcreep extensometer	40

LIST OF TABLES

Table		Page
1	Analysis of second phase particles in X-520 beryllium	14
2	X-ray analysis of selected second-phase particles in X-520 beryllium	15
3	Analysis of second phase particles in HIP 50 beryllium	23

SECTION 1

INTRODUCTION

Advanced generations of inertial instruments require that induced long-term microplastic strains be maintained at levels substantially lower than 10^{-6} to 10^{-7} inch/inch. Strains of this low order of magnitude are expected to occur in moderate strength engineering materials with the application of very low applied stresses like those that are associated with essential assembly operations such as shrink fit, bolt tension, or rotational stress. These externally applied stresses are the most difficult to control in that some minimum elastic stresses need to be applied to the different structural members when the instrument is assembled for satisfactory functioning of the instrument. The gradual relief of such applied elastic stresses, with the passage of time, results in permanent shape changes in the material (giving rise to mass shifts) because of the induced plastic strain. These changes manifest themselves in small amounts of mass shifts which become sources of error in the performance of the inertial devices.

The sources of dimensional instability are several, among which some readily identifiable ones are phase transformation, relief of residual stresses, and microplastic deformation (occurring because of externally applied stresses) that was discussed above. Dimensional changes related to phase transformations and residual stress relief processes (unlike those related to externally applied stresses), can be substantially minimized (if not altogether eliminated) by appropriate material and process selection procedures.

Because it is not possible to reduce these stresses below a reasonable limit, it becomes desirable to predict the plastic micro-strain in such circumstances and compensate for the resulting errors.

In the past, much of the prediction criteria for the several instrument component members has been based on the use of the measured microyield strength (MYS) of the material. More recently, however, it has become apparent that microcreep, which is a continuous dimensional change measured at a 10^{-6} or lower strain level at a given temperature and applied load, is of considerably greater significance to the designer than is the MYS of the material which appears only suited to short-term strain effects.[(1)*] Observations elsewhere[(2)] have shown that significant microcreep will occur at stress levels that are but only a fraction of the measured MYS value.

The emphasis in this activity has progressively shifted from a determination of the MYS value of the HIP-50 beryllium material to an examination of other experimental grades of beryllium. In particular, the X-520 grade of beryllium produced by the Brush-Wellman Co. has been examined for MYS in a manner analogous to the HIP-50 beryllium. A close examination of the microstructure of the several beryllium samples using standard analytical techniques has continued with the aim of being able to explain the effects of selected heat treatments on the measured micromechanical properties of the different grades of beryllium. Earlier efforts at determining sample microstructures using X-ray and microscopic techniques have been supplemented with detailed transmission and scanning transmission electron microscopy (TEM/STEM) evaluations of the as-processed and heat treated HIP-50 and X-520 materials. These additional determinations are included in this report. Substantial progress has been made on the development of an in-house capability for measuring long-term tension microcreep at the 10^{-7} inch/inch level and this is discussed. Also included is a description of results obtained using finite element modelling techniques for predicting actual material behavior from the measured rates of microcreep.

---

* Superscript numerals refer to similarly numbered items in the List of References.

SECTION 2

OBJECTIVES

The present objectives of this program are [illegible]llows:

(1) To study the microplastic behavior of HIP-50 and X-520 grades of beryllium and its relationship to microstructure.

(2) To predict microdeformation behavior of typical instrument components using finite element analysis techniques and experimentally determined microcreep data.

(3) To investigate the suitability of metal-matrix composite materials as alternate materials to beryllium as the structural members of the inertial devices.

SECTION 3

PREVIOUS WORK

Work accomplished prior to this past year's effort is described in detail in References 1, 3, 4, and 5. A brief summary is included here.

(1) Procedures were established for preparing specimens and measuring values of their microyield strength (MYS) while ensuring that a reasonable precision of alignment was obtained.

(2) MYS and macroyield strength measurements were performed on as-received and heat treated hot isostatically pressed HIP-50 beryllium produced by Kawecki Berylco Industries. Similar evaluations were also performed on as-pressed and heat treated samples of the hot pressed X-520 beryllium grade experimentally produced by the Brush-Wellman Co. Significant differences were observed in the MYS characteristics of these two beryllium grades, even though their macro properties were quite comparable.

(3) The MYS measurements showed that if a correlation is desired between the processes of microyield and microcreep one must take into account the value of the strain exponent in the low strain regime (obtained by plotting the data on logarithmic coordinates) in addition to the measured MYS value.

(4) Optical microscopy was determined to be of limited utility in determining the effects of the several thermal treatments on sample microstructure. It was concluded that extreme

care was needed in sample preparation for microstructure examination to avoid introducing damage in regions near the surface.

(5) Transmission electron microscopy was determined to be a substantially more powerful tool for examining sample microstructure. Initial examinations of the as-HIPed material were made at the National Bureau of Standards using a perchloric-based solution. Subsequent examinations were performed on heat treated HIP-50 samples at a local facility using a chromic-acetic solution which was successfully investigated for this purpose. The differences noted in the samples were related mainly to phase precipitation and segregation.

(6) Scanning electron microscopy (SEM) performed on fractured surfaces of HIP-50 and X-520 samples showed a few regions in the X-520 material that appeared less crystalline than the surrounding material. X-ray analysis showed that these regions contained higher levels of silicon, oxygen, and aluminum. Long-term Debye-Scherrer exposures of the several samples showed extra X-ray diffraction peaks associated with the X-520 samples which were attributed to the formation of the compound Be_2SiO_4.

(7) Modelling studies were performed on a typical gyro component and on a disc-shaped specimen for biaxial loading. Deflection, resulting from microcreep processes, was calculated for these instances. Finite element analytical techniques were also used for evaluating the stress field in a proposed test specimen for microcreep measurements. It was determined that if three individual lugs were used to replace the axisymmetric ribs of a conventional tensile microcreep sample, a substantially more uniform stress field is obtained.

(8) A reasonably extensive effort was expended on the design of an experimental piece of apparatus for measuring microcreep at the 10^{-7} inch/inch level. The system was designed to accommodate the application of load in the range of 100 to 10,000 $lb/in.^2$ with test runs that allow sample temperature to be maintained at a given value between 100 and 180°F, regulated to within ±0.02°F.

SECTION 4

PRESENT WORK

Work accomplished during this past year has included a further detailed microstructure characterization of the HIP-50 and X-520 beryllium grades and interpretation of their measured mechanical properties with respect to these observations. A substantial level of progress was achieved in the design, fabrication, and assembly of a 10^{-7}-inch/inch microcreep measuring facility, which is to be used to generate experimental microcreep data on beryllium for research as well as engineering purposes. Use of the finite element modelling technique for predicting the microdeformation of typical instrument parts from experimentally obtained microcreep data has continued. Most of the microcreep data used so far have been collected on I-400 instrument grade beryllium at the National Bureau of Standards (NBS) under a parallel program, which is also supported by the Office of Naval Research. (The Charles Stark Draper Laboratory, Inc., serves as a source of applications information to NBS and has provided the specialized beryllium machining facilities for manufacturing of the microcreep specimens.)

4.1 Microstructure Evaluations

Earlier attempts at examining these beryllium materials using optical microscopy had demonstrated the minimal utility of this technique in defining the microstructure of the material. It had, nevertheless, assisted in the determination of the grain structure and had also indicated that considerable care was needed during sample preparation because of the likelihood of incorporating into the microstructure mechanically induced artifacts. To avoid this, considerable care should be exercised over the processes of machining, sectioning, grinding, and lapping of the beryllium surface.

To gain further information on the finer microstructure details of the material, transmission electron microscopy (TEM) was attempted on as-HIPed and heat treated HIP-50 samples and this technique was determined to be a considerably more powerful tool for sample characterization. Differences in second phase precipitation distribution were observed among the several samples. However, using the conventional TEM technique it was not possible to identify the chemical species that were present in the second phase particles. Subsequent long-term X-ray Debye-Scherrer exposures on the as-pressed and heat treated HIP-50 as well as the X-520 materials revealed the existence of extra lines in the X-520 samples that were absent in the HIP-50 samples. These extra lines were attributed to the phase Be_2SiO_4. Here too, however, even though differences were observed between samples belonging to the two grades of beryllium, there was no apparent distinction that was observable between samples belonging to a given beryllium type even though these had been subjected to different heat treatments prior to examination. As a consequence, we have now performed a considerably more detailed analysis of the second phase particles in these materials by combining the TEM technique with the more recently developed scanning transmission electron microscopic (STEM) technique to obtain chemical information on the second phase particles in addition to information on their size and distribution.

4.2 Sample Preparation for Electron Microscopic Examination

Because of the likelihood of inducing excessive mechanical damage during the preparation stages of the TEM samples (if proper care is not exercised), a reasonably gentle procedure has been developed and was found to be quite satisfactory for this purpose. This procedure consists of slicing a 0.020-inch-thick beryllium slice from rod stock using electrical discharge machining (EDM) and then coring 3-mm discs from the thin slice, also using EDM. The disc samples are then rigidly mounted on a reasonably flat surface and the exposed surfaces gradually ground on progressively finer silicon carbide abrasive papers while taking care to ultrasonically clean the surfaces after each operation.

The thickness of the sample is reduced to about 0.010 inch with these operations which are performed using papers of grit sizes 240, 320, 400, and 600, respectively. The ground surfaces are next lapped using 6- and 3-μm diamond paste followed by additional polishing using 0.3- and 0.05-μm Al_2O_3 particle suspension in water. These lapping operations involve polishing of the surface for roughly two to three minutes with each medium and all of this results in the production of surfaces that possess a metallurgically polished appearance. The samples are removed from the mount and the remaining surface is exposed and polished in an identical manner. This results in samples which are about 0.002 to 0.003 inch thick and ready for further thinning using electrochemical means. Samples are typically stored prior to the jet-thinning step glued onto glass slides with DiOctyl Phthalate. The final thinning of the sample has been accomplished with a dual-jet electropolishing procedure. The electrolyte that was used for this work consisted of 60% phosphoric acid, 35% glycerol, 2.5% chromic acid, and 2.5% water. The applied potential was 30 volts.

4.3 TEM/STEM Studies

A JEOL 200CX electron microscope was used for performing the conventional TEM analysis and a Vacuum Generators HB-5 unit was used for the STEM work. The chemical composition analysis that was performed on the second phase particles in the STEM was made possible by employing an energy dispersive X-ray analyzer which detected the X-rays that were generated from these particles. Two different X-ray detectors were used, one of which had an ultra-thin energy window and was capable of detecting oxygen. Detailed analyses were performed on as-pressed and heat treated X-520 as well as HIP-50 samples. Analyses were performed with respect to particle size, density (number of particles per unit volume), distribution, and chemical composition.

4.4 X-520 Beryllium

Figure 1 is a low magnification, dark field detector image from an as-received (which is also the as-pressed) X-520 specimen.

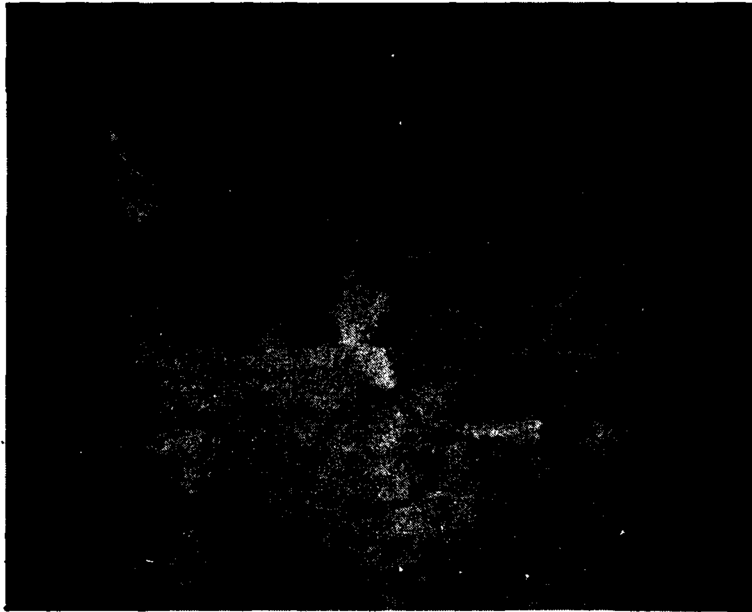

4/82 CD27245

Figure 1. Annular dark-field image in stem showing second-phase particles and grains in as-received material.

The micrograph clearly shows the presence of the second phase particles, which appear in dark contrast, distributed throughout the material. Most of the particles were observed at the grain boundaries; however, a significant fraction of the particles, n this sample, also appeared to be located elsewhere in the beryllium matrix. Similar, low magnification observations were also made on the other specimens, which were heat treated under a variety of conditions. These heat treatments, identified as HT1, HT2, and HT3, were reported earlier.[1] The observations made on the heat-treated specimens were similar to those observed in

Figure 1, except that the second phase particles were less uniformly dispersed in the heat treated specimens with a larger majority of them segregating preferentially at the grain boundaries. Using images of the type shown in Figure 1, Table 1 was constructed with respect to data obtained on these second phase particles. The data were obtained primarily for differences in these samples with regard to size, distribution, area fraction, and spatial density of the second phase particles. A reasonably large number of particles was examined for this purpose.

All of the heat treated specimens showed an average particle size of about 0.1 μm as compared to the as-received sample which had an average particle diameter of roughly 0.25 μm. The increase in the density of particles in the HT1 and HT3 samples was interpreted as indicative of increased precipitation in the beryllium alloys. This additional precipitation might well have contributed to a lowering of the measured average particle size as well as resulting in a greater preference for the grain boundary segregation that was observed in these samples.

Besides considerations relating to size, distribution, and number density of the second phase particles, many of these were also examined for elemental analysis using the STEM. The data that were collected for several arbitrarily selected particles in the different samples are shown in Table 2. As stated earlier, the presence of oxygen in the particles was detected using an ultra-thin-window, energy-dispersive detector. The analysis for oxygen presence was performed on the particles present in the as-received and in the HT2 heat treated samples. Huge oxygen signals were measured from all of the particles that were examined, indicating that mostly all the particles present in the X-520 materials contained large amounts of oxygen. It was also noted that silicon and iron were also invariably present (in addition to oxygen) in all the particles that were analyzed. Other elements, including aluminum, phosphorus, sulphur, and chromium, were found to be only occasionally present. The capability for detecting beryllium was not present with this instrumentation.

Table 1. Analysis of second-phase particles in X-520 beryllium.

Descriptor / Sample (Heat Treatment)	Image Magnification	Number of Particles	Σ Particle Area (mm^2)	Area Fraction (%)	Number Density (Particles/cm^3)	Average Particle Diameter (μm)
5 (As-Rec'd.)	2,000	525	113.43	1.2	0.8×10^{12}	0.26
6 (HT1)	10,000	174	173.54	1.8	7.2×10^{12}	0.11
8 (HT2)	20,000	41	128.18	1.3	6.8×10^{12}	0.10
7 (HT3)	10,000	437	504.74	5.2	18×10^{12}	0.12

HT1: HIP + 600°C, 100 h

HT2: HIP + 1055°C, 2 h solutionize, quench + 370°C, 24 h, furnace cool

HT3: HIP + 870°C, 2 h + slow cool and step age (750°C, 20h + 720°C, 20 h + 695°C, 20 h, furnace cool)

Table 2. X-ray analysis of selected second-phase particles in X-520 beryllium.

SAMPLE		ELEMENT						
No.	Location	O	Al	Si	P	S	Cr	Fe
5	B1	VS	S	S	-	-	-	S
5	C1	VS	W	W	-	-	-	S
5	D1	VS	W	W	-	-	-	S
5	E1	VS	-	W	-	-	-	-
5	F1	VS	VS	S	-	-	W	VS
5	G1	VS	-	W	-	-	-	-
5	H1	VS	-	-	-	-	-	-
6	A	ND	-	W	-	-	-	W
6	B	ND	-	-	-	-	-	W
6	C	ND	W	S	-	-	W	S
6	D	ND	W	W	-	-	-	W
6	E	ND	S	VS	W	-	-	S
6	F	ND	-	W	-	-	-	W
6	G	ND	-	W	-	-	-	W
6	H	ND	-	-	-	-	-	W
6	I	ND	-	W	-	W	-	W
6	J	ND	-	S	-	W	W	S
7	A	ND	W	S	W	-	-	S
7	C	ND	-	S	S	S	-	W
7	D	ND	-	W	W	-	-	W
7	E	ND	-	W	-	-	-	W
7	F	ND	W	S	S	W	-	S
7	G	ND	-	S	S	S	-	S
8	A	VS	W	S	S	-	-	W
8	C	VS	-	S	S	-	S	S
8	D	VS	W	S	S	W	-	S
8	F	VS	W	W	-	-	-	W
8	G	VS	W	S	S	S	S	S
8	I	VS	W	VS	W	W	S	VS

NOTES: VS=Very Strong, S=Strong, W=Weak, -=No Peak, ND=Not able to be Detected

These oxygen-related observations clearly showed that precipitates consisting of binary and ternary compositions of beryllium, aluminum, and iron such as those reported to be present in instrument grade, I-400 beryllium,[6,7] are not present in detectable quantities in the X-520 materials. The observations were in agreement with X-ray diffraction results reported earlier on as-pressed and heat treated X-520,[5] which had shown the presence of extra lines attributed to the Be_2SiO_4 phase composition. The STEM analysis, however, did show that the particle composition itself was substantially richer in oxygen than would be expected for stoichiometric Be_2SiO_4. A typical STEM analysis performed on a second phase particle in the as-pressed specimen is shown in Figure 2. The implication of these observations, therefore, is that the bulk of an individual particle must still be BeO with some reacted regions consisting of the Be_2SiO_4 phase. Silicon is believed to assist in the agglomeration of the BeO particles. It is possible that the formation of this orthosilicate phase is a result of such a process. The presence of iron can be explained as being associated with a small solubility of iron in the BeO particle.

These observations, to some extent, also appeared to correlate with the earlier SEM examination of the fractured surface of the X-520 material that had shown what appeared as a region possessing less crystallinity than the beryllium matrix. Using X-ray mapping of this region it was determined, as reported earlier, that there was a greater concentration of the elements silicon, oxygen, and aluminum in this area as compared to the surrounding beryllium. Iron concentration, however, was not detected using the mapping procedure. It is likely that the indicated absence of iron concentration in that region (which is indicated to have been present based on current results) was due to a similarity in the dissolved level of iron in the particles and in the surrounding matrix. The presence of aluminum observed in the SEM can be explained by the STEM observations shown in Table 2 in that it was frequently (if not always) found to be present in the particles.

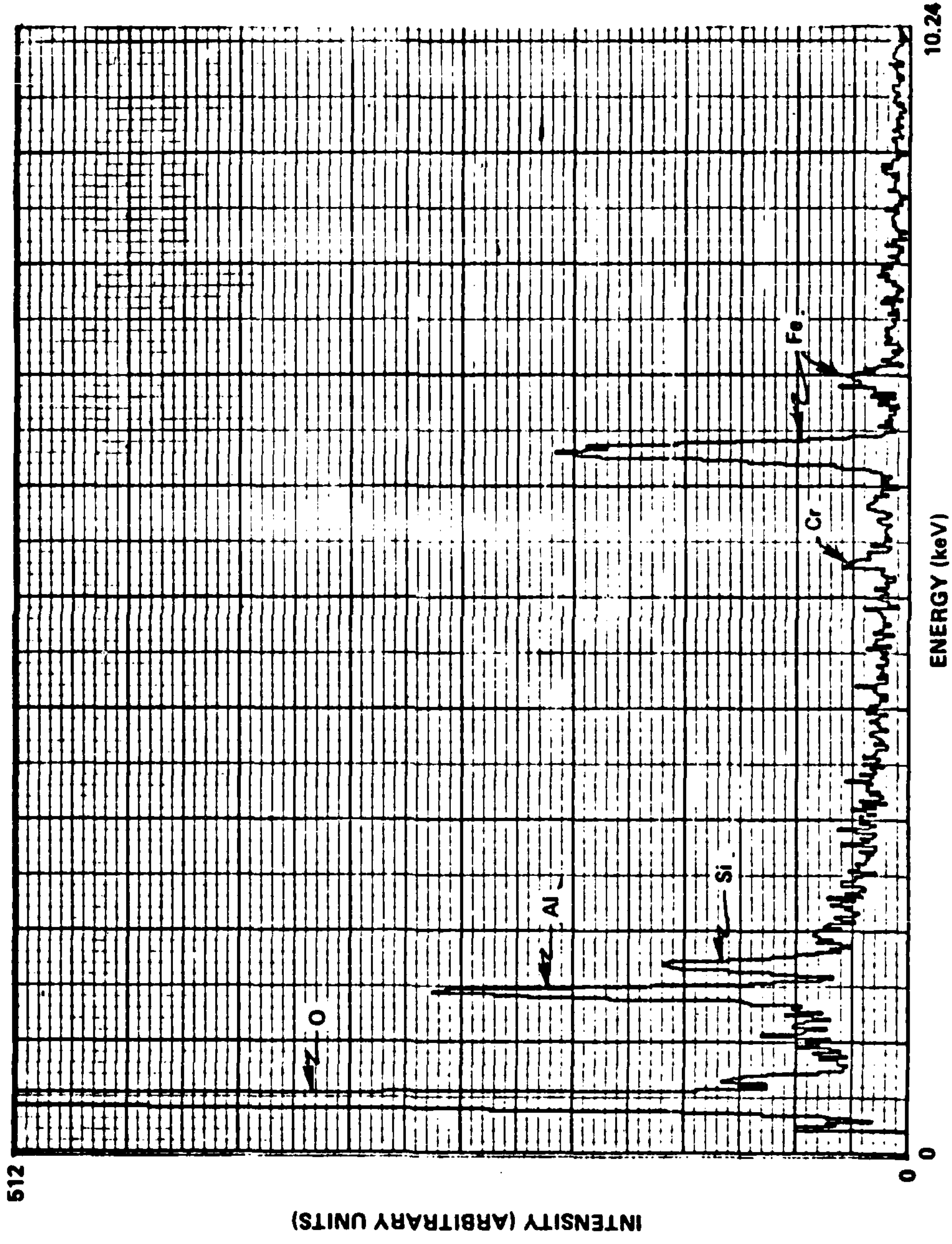

Figure 2. (X-ray) signal from large precipitate in as-received X-520 sample.

It should be noted, however, that TEM examination has shown these particles to be composed of crystalline material and the reason why the SEM observed region appeared less crystalline than the beryllium matrix is believed to have resulted from the very small size of the second phase particles that were present (0.1 to 0.26 μm average) compared to the much larger grain size of beryllium (about 10 μm).

4.5 HIP 50 Beryllium

Figures 3 through 6 are representative of as-HIPed and heat treated HIP 50 microstructures as observed in the electron microscope. The observations that were made during this study, for the most part were quite similar to what was reported earlier;[1] however, a more detailed analysis of the second phase particles was attempted in this work to quantify the data in a manner similar to what was done on X-520 beryllium. The results of this effort are tabulated in Table 3.

Briefly, the following observations were made with respect to the microstructure of the as-HIPed and heat treated specimens.

(1) As-HIPed

The average grain size was larger in this specimen than what was observed for most of the other samples. Essentially, only high angle grain boundaries were observed in this condition. Most of the second phase particles were located at the grain boundaries with the grain interiors appearing relatively clean. A low density of particles was observed to be uniformly dispersed throughout the sample.

(2) HT1

The interiors of this sample were very clean. This sample, however, unlike the other specimens, was from a different lot of HIP 50. Again, most of the particles were located at the grain oundaries even though several boundaries were found to be reasonabiy cl ar of precipitates.

Figure 3. As-received HIP 50. TEM micrograph.

1cm = 0.67μm

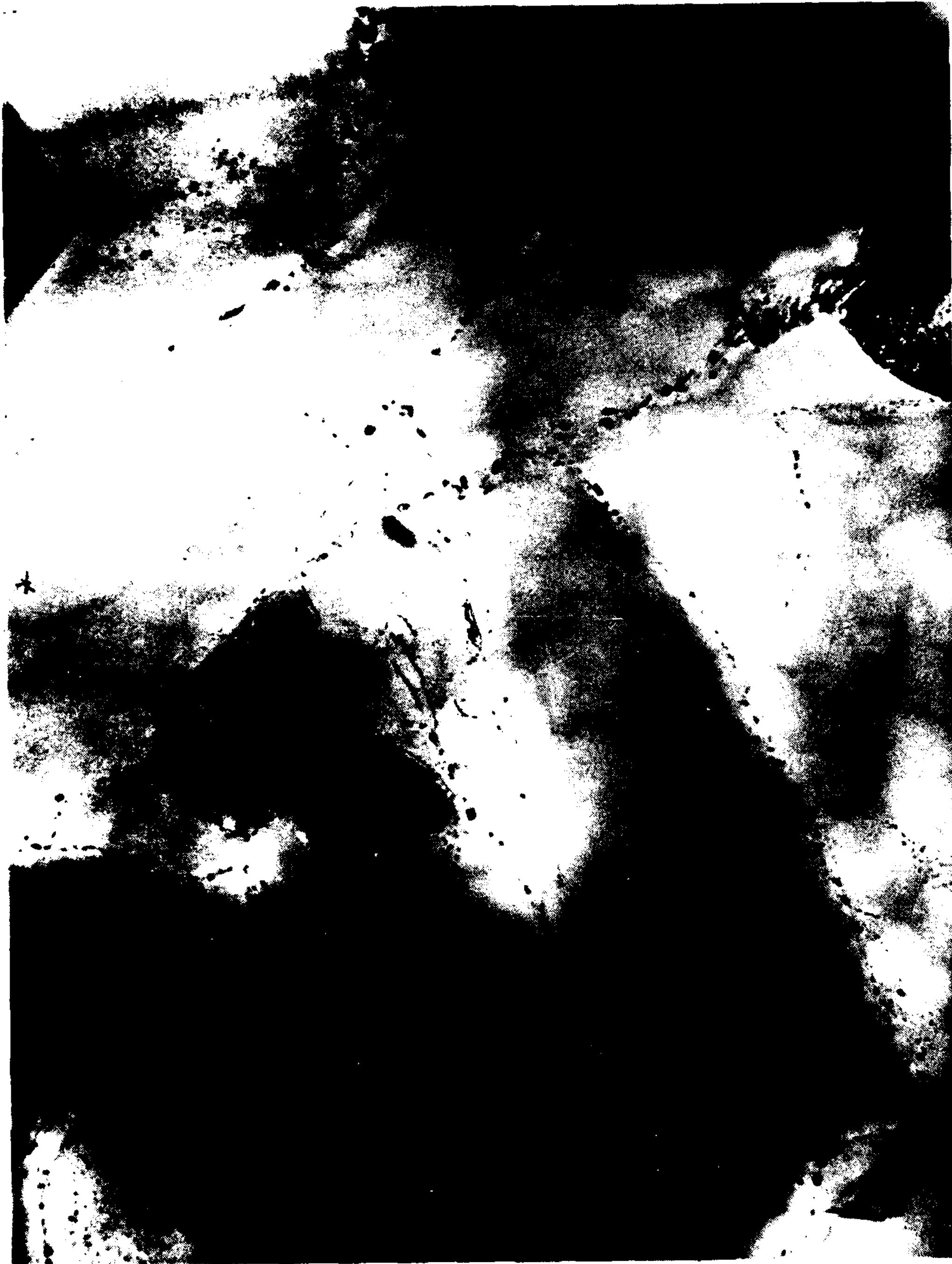

Figure 4. HT1-treated HIP 50. TEM micrograph.

← 0.42μm →

Figure 5. HT2 treated HIP50. TEM micrograph.

0.4μm

Figure 6. HT3 teated HIP 50. TEM micrograph.

← 0.3μm →

Table 3. Analysis of second-phase particles in HIP 50 beryllium.

Descriptor / Sample/ Fig. No.	Heat Treatment	Image Magnification	Number of Particles	Σ Particle Area (mm^2)	Area Fraction (%)	Number Density ($particles/cm^3$)	Average Particle Diameter (μm)	Average Grain Size (μm)
3A	As-rec'd	15,000	96	43.5	1.4	0.29×10^{14}	0.05	7
HIP 50*	HT1*	24,000	273	121.7	1.2	0.52×10^{14}	0.03	4
2A (Fig. 5)	HT2	25,000	136	160.75	5.1	1.13×10^{14}	0.05	5
3B (Fig. 2)	HT3	35,000	64	172.0	6.9	1.05×10^{14}	0.05	5

*Sample from a different lot of HIP 50

HT1: HIP + 600°C, 100 h

HT2: HIP + 1055°C, 2 h solutionize, quench + 370°C, 24 h, furnace cool

HT3: HIP + 870°C, 2 h + slow cool and step age (750°C, 20 h + 720°C, 20 h + 695°C, 20 h, furnace cool)

(3) HT2

As with the previous specimens, the majority of the second phase particles appeared at the grain boundaries. The number density of the particles as shown in Table 3 was the highest for this sample. Several grain boundaries were found to be free of particles.

(4) HT3

In this sample, even though most of the particles were located at the grain boundaries, many low angle grain boundaries were observed that were found to be free of the particles. As indicated in Table 3, the number density of the particles was reasonably high even for this sample.

4.6 Comparison of X-520 and HIP 50 Microstructure Data

Analysis of the second phase particles in HIP 50 beryllium has shown these to be composed primarily of the oxides of beryllium. This differs from the particles in X-520, which contained reacted regions of the Be_2SiO_4 phase, and many of which were found to contain iron, possibly in solid solution. The HIP 50 average particle size (as shown in Table 3) was typically one-half of what was observed for X-520, while the number density of particles in HIP 50, in general, was substantially larger than what was observed for X-520. This was generally expected because the total oxide levels for HIP 50 (~ 1.7% BeO) and X-520 (~ 2.3% BeO), as reported earlier,[5] are reasonably comparable, and for finer particle sizes (in HIP 50 compared to X-520) one would expect a larger number of particles in a given volume of material. These observations also showed that differences existed within specimens heat treated differently from a given beryllium grade. However, the differences between the two (X-520 and HIP 50) beryllium grades appeared to be more significant, principally because the TEM samples were obtained from material removed from only one sample representing a given heat treatment condition, and this type of data could conceivably be discolored by spatial inhomogeneities in composition that might exist in these materials. However, since certain

aspects such as second phase particle composition, size, and number density were substantially different for one grade of beryllium with respect to the other (as indicated collectively by all the samples that were examined), these differences were deemed significant and considered important for purposes of explaining the micromechanical property differences that were earlier observed between the two beryllium grades. The grain size in these samples appeared to be reasonably comparable and, therefore, possibly not very significant.

4.7 Correlation of Microstructure with Microyield Behavior

MYS measurements reported earlier[1,5] had shown that the HIP 50 grade of beryllium was substantially superior in its MYS value compared to the X-520 grade. The latter, however, had shown a substantially greater level of strain hardening characteristic (as indicated by the measured strain hardening exponent) than the HIP 50 samples. Because it appears to be quite desirable to have both a high MYS value as well as a high strain hardening exponent for developing a maximum resistance to microcreep processes, it is important to understand their dependence on the microstructure of the material.

The TEM/STEM results (discussed earlier) show a much finer particle size and a higher number density of the second phase particles in HIP 50 compared to the X-520 grade. In both these grades of beryllium, the second phase particles are mainly segregated at the grain boundaries. The foregoing would therefore suggest that the finer particle distribution of HIP 50 is responsible for the high MYS that is measured. This would further imply that initiation of microplastic deformation in these materials occurs primarily in the grain boundary regions, since these are expected to be strengthened (by the fine particles that are distributed) to a larger degree in HIP 50 than in X-520. The lower level of strain hardening observed for HIP 50, in comparison with X-520, can be attributed either to a lowered level of solid solution strengthening of the grain interiors (associated with its higher level of purity) or to the presence of the very high level of stresses that are needed to initiate the microplastic flow process as indicated by the measured MYS value.

The coarser distribution of the second phase particles observed in X-520 is believed to have resulted from: (1) the presence of an excessive amount of silicon, which has apparently aided the agglomeration of the oxide, thereby accounting for the existence of reacted Be_2SiO_4 regions in the BeO particles, and (2) the possible use of a higher temperature during consolidation with hot pressing. Since much higher pressures are available during hot isostatic pressing, the HIP 50 materials were possibly densified at a lower consolidation temperature.

The implication of the foregoing appears to be to keep the level of silicon low in the material. Silicon is a desirable constituent in beryllium produced by hot pressing because it aids in the densification process. However, if the process of HIP is used for consolidation, the silicon can be dispensed with and the densification performed at temperatures substantially lower than are required for hot pressing. All of this should result in the production of beryllium with a fine particle distribution in the grain boundary regions similar to what was observed for HIP 50 beryllium. The lower temperatures of HIP would also inhibit thermally activated grain growth in addition to minimizing particle agglomeration. The use of impact attritioned powder, such as what was reportedly used for fabrication of HIP 50, is also expected to impact favorably on the overall properties. Surface cracks and fissures will occur in powder particles produced by this method, which will develop an surface oxide film, and when these flaws heal under the effects of temperature and pressure, during consolidation, fine particle distributions are also expected to occur deeper in the grain interiors.

The role of impurities other than silicon in X-520 is less clearly defined. Iron apparently is not significant because it is found to exist in similar amounts in both the beryllium grades (see Table 1 in Reference 5). Aluminum and carbon, however, are higher in X-520 than in HIP 50. It is conceivable that if solid solution strengthening of the grain interiors is responsible for the increased strain hardening measured for X-520, then aluminum is responsible for the observed effect.

4.8 Microcreep Modeling

Previous work[4] at CSDL has shown that modeling of instruments using an existing finite element code allows performance prediction if accurate creep laws are known. Results to date from NBS have been limited to NBS's 10^{-7}-inch/inch apparatus, and at relatively high stress. On this basis a creep law of the form

$$\varepsilon = \varepsilon_{op} + A\ln\left(1 + \frac{t}{B}\right)$$

where ε = total creep strain

ε_{op} = instantaneous plastic strain

A = constant (nondimensional)

t = time (hours)

B = constant (hours^{-1})

has been proposed.[2]

The rate of change of creep is then given by

$$\frac{d\varepsilon}{dt} = \frac{A/B}{1 + t/B}$$

Evaluating this slope at 1000 and 10,000 hours at the stress levels tested gives:

Stress (lb/in.^{2})	A	B	$\frac{d\varepsilon}{dt}\left(\frac{\mu inch}{inch\text{-}hr}\right)$ at 1000 hours	$\frac{d\varepsilon}{dt}\left(\frac{\mu inch}{inch\text{-}hr}\right)$ at 10,000 hours
3000	0.110	1.21	1.099×10^{-4}	1.1×10^{-5}
10,000	0.162	0.069	1.62×10^{-4}	1.62×10^{-5}
15,000	0.328	0.165	3.279×10^{-4}	3.3×10^{-5}
20,000	0.196	0.014	1.96×10^{-4}	1.96×10^{-5}

A detailed finite element analysis of gyro members has shown that the largest beryllium stresses are caused by assembly joining methods such as shrink fits and torque nut loads. These stresses could produce instrument drifts due to stress relaxation. However, at least 1000 hours elapses between the time of assembly and when the instruments are tested. At the creep rates predicted (with the NBS creep law) after 1000 hours, no detectable instrument drifts would be observed. Each time the instrument is made operational, lower level stresses are created by wheel speed and thermal gradients (less than 1000 $lb/in.^2$). These stresses have yet to be tested, and therefore no firm conclusions with respect to instrument drift related to beryllium microcreep can yet be reached.

4.9 Development of Instrumentation for Microcreep Measurement

During this past year, the CSDL-designed 10^{-7}-inch/inch microcreep tensile testing facility has been built according to very stringent requirements. Several iterations of design have evolved that should improve the soundness and sensitivity of this mode of measurement. In addition, new technology has been gained in the application of a sputtered insulating film onto a large beryllium surface. Overall, the success of the facility will depend on the practicality of the design philosophy, which can be considered in several categories: load train, specimen design, capacitive extensometer, testing environment, and signal instrumentation.

The system is shown in Figure 7. The Applied Test Systems' Tester (12K pounds capacity) is in the lever arm mode (ratio 10:1) and it is applying a load of 10 KSI through the in-house developed load train to the specimen. The oven is awaiting the installment of a platform at the date of this photograph. All the supportive electronics sit on the left of the tester.

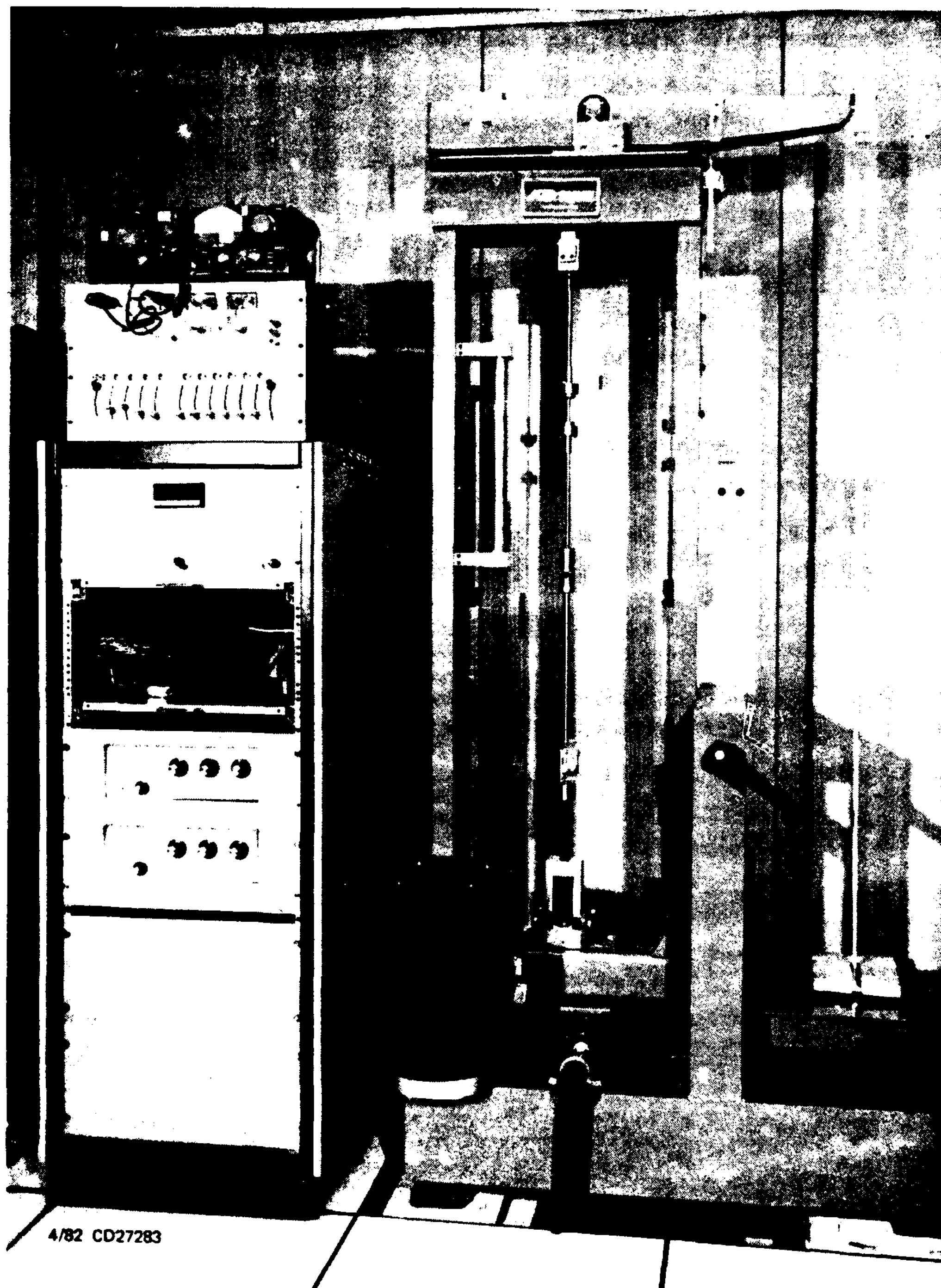

Figure 7. CSDL designed/microcreep testing apparatus.

The load train is aligned with two commercial knife-edge couplings of 6000 pounds capacity. A BLH load cell with a rated output of 3mV/V ±0.10 percent and a nonlinearity of 0.05 percent of the rated output has been installed in line to give accurate, direct readings of applied load. This feature is particularly necessary for the lever arm mode with which the constancy of the load is dependent on the levelness of the lever arm, which can change with temperature and metal relaxation.

The underlying philosophy for the load train is that once the initial alignment is made, the only change to occur during a test run should be to the specimen. It is for this reason that the load train has been designed and fabricated by CSDL as shown in Figure 8. The pull rods were rough-machined, stress-relieved, and ground to ensure maximum straightness. The coupling between the pull rods and specimen is made through a bronze ball and a steel socket arrangement. Both were lapped together to ensure minimum contact friction for the required supportive strength. The radial centering of the specimen is done with a split ring which holds and centers it within the ball and socket.

Two modes of operation are required to apply the wide range of stresses needed. The lever arm mode is best suited for loads in the 3 to 20-KSI range while the dead-load mode is more accurate in the 100 to 3000-lb/in.^{2} range. Conversion from one mode to the other is made through connections below the lower pull rod. This keeps most of the instrumental errors common to both modes.

The specimen design incorporates two three-lug systems to which the extensometer is attached, as shown in Figure 9. Finite element analysis has indicated that the reduction to this scheme from the full axisymmetric rib reduces the interference stress field in the specimen by a factor of five. Three lugs have also been found to be sufficient to support the extensometer weight.

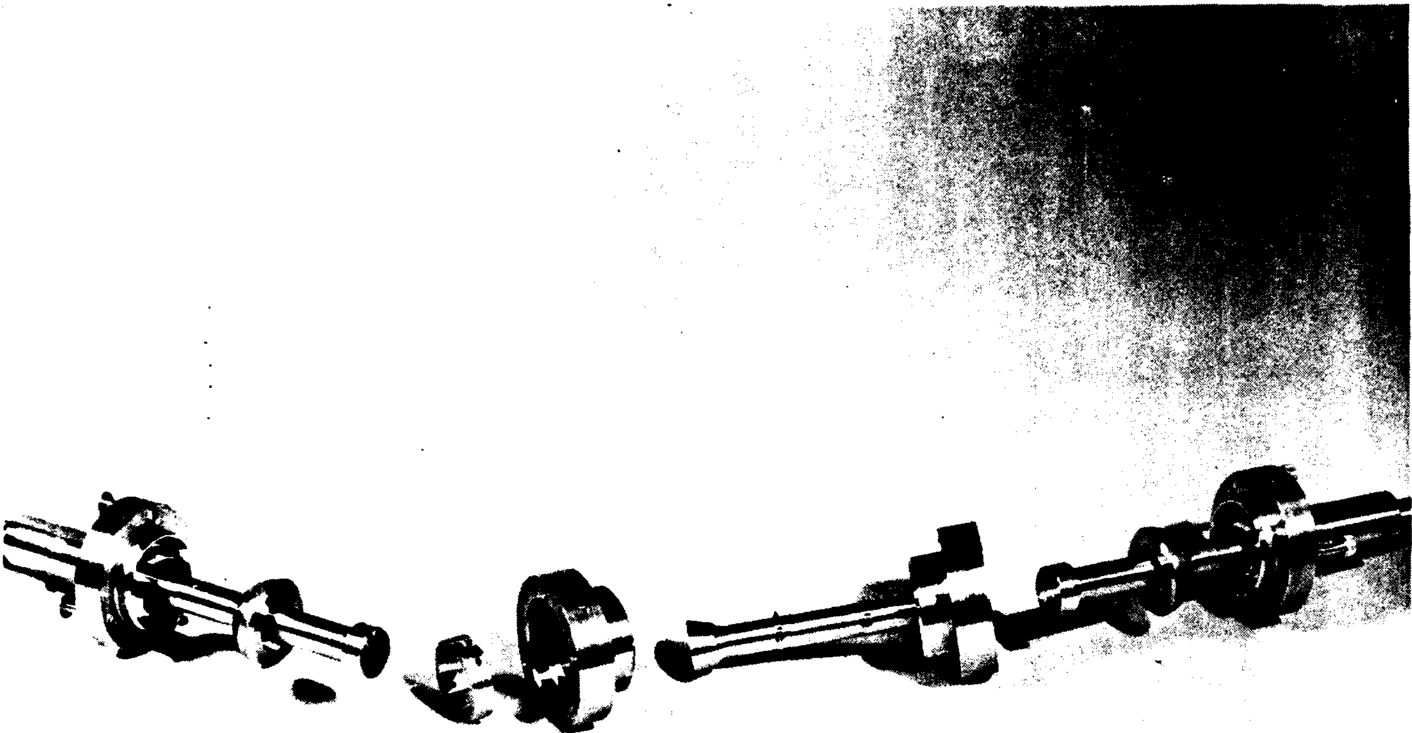

Figure 8. Load train for microcreep measurement.

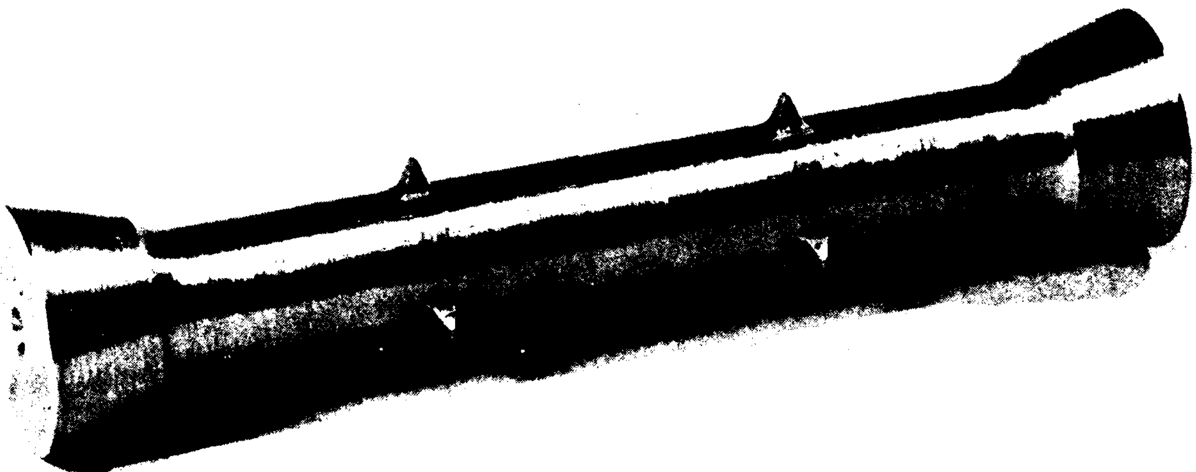

Figure 9. Typical microcreep specimen.

The chronology and identification of each specimen is recorded from the date of material acquisition through all processing steps until it is tested. This information may be useful if it is suspected that processing parameters are affecting specimen-to-specimen results.

The machining of specimens is done in a controlled manner similar to the way all other beryllium hardware is fabricated at CSDL. From the as-received state, the steps are as follows:

(1) Rough machine the beryllium shape allowing 0.005 to 0.015 inch over the finish size.

(2) Stress-relieve the part in a vacuum or inert atmosphere by heating it to a temperature of 1450° ±20°F and retaining it at that temperature for a period of one hour.

(3) Cool the part in the oven to 400°F at a maximum rate of 100°F per hour. (A vacuum or inert atmosphere is not required at temperatures below 700°F.)

(4) Still-air-cool the part at room temperature.

(5) Final machine the specimen.

(6) Heat the part to a temperature of 210° ±10°F and hold for a period of 10 minutes.

(7) Cool to 70°F ±5°F and hold for 10 mintues.

(8) Cool to -100°F ±10°F and hold for 10 minutes.

(9) Repeat (6) through (8) for a total of five thermal cycles.

The capacitive extensometer is of a novel concept and consists of three I-400 beryllium disks approximately three inches in diameter. Two of them are attached to the three-lug sets which define the gage length. The third is situated between the other two and is free to move up and down through the adjustment of micrometer spindles which are attached to the lower disk. Along with the upper disk it defines the working gap of the capacitor. Both contain thin-film nickel plates which were sputter-deposited onto them.

The disk material was chosen to be beryllium for its good thermomechanical match to the specimen. Its small mass density is also favorable to the three small lugs which support it. The planarity of the disks when attached to the specimen is ensured by the tongue and groove design shown in Figure 10. The lugs are mated to the disk groove after their angles have been custom-matched, and the mating is done with very little torque so as not to deform the groove.

The method of formation of the capacitive films required some development. It was decided that sputter-deposited films afforded the best quality and bonding strength. In addition, the deposition temperature should be maintained below 250°C to avoid distorting the disks. Based on the minimum surface roughness achievable by lapping and the dielectric of choice, SiO_2, the thickness of 12,000 Å was decided upon to give good coverage and a minimum breakdown voltage in excess of 10 times the operating voltage of 30 volts. Since pinhole formation in the insulating film is not always avoidable, it was necessary to apply the coat in two 6000-Å steps with an exposure to air and a cleaning step in between. Prior to the deposition of the nickel, the SiO_2 film was carefully inspected to be clear of pinholes. (Otherwise, it would easily lead to a breakdown rendering it useless.) SiO_2 was also chosen for its resistance to scratching and cleaning solvents. The electrical leakage resistance of the film was tested to be about 500 megohms with 500V applied across it.

Figure 10. Capacitive extensometer plates.

The capacitive plates are a 12,000-Å-thick sputter-deposited film of Ni-7% Va. The mixture renders the film nonmagnetic. Photolithography was used to define the capacitive plate patterns on the two disks. The unwanted nickel was then removed chemically. The patterns are shown in Figure 11. The pads which extend onto the beveled edge are for soldering short electrical leads which terminate on the opposite side of the disk at a more rigid connector wherefrom a shielded coaxial wire continues to the electronics. The three capacitive plates on one disk are intended to give separate readings 120 degrees apart to detect bending motion if it is desired.

The testing environment is comprised of a room with temperature and humidity control that is also vibration-free. This is important for keeping the electronic instrumentation and tensile tester stable over long periods of time. The local environment about the specimen will be controlled by the oven, which will also be in use in room temperature work so as to be electrically common to the extensometer for all temperatures. The full extensometer is also within the oven so that it will be at the same temperature as the specimen. A proportional-type controller will hold the system to ±0.02°F regulation within the testing temperatures of 90° to 200°F. The oven is of a cylindrical design and consists of three shells of aluminum separated by closed-cell neoprene insulation. It is mounted on a platform which can be raised and lowered smoothly with a manual crank to allow access to the extensometer. A photograph of the oven is shown in Figure 12 and a schematic showing the monitoring and controlling features in Figure 13.

The signal instrumentation consists of a General Radio type 1620A Capacitive Measuring Assembly with 10^{-11} μf resolution and 0.01 percent accuracy, which gives capacitive readings through null detection. A phase-locked amplifier can also be used in conjunction with this system to give a dc voltage output proportional to the plate separation. The working air gap will be about one mil. The schematic showing the full instrumentation and the extensometer assembly is given in Figure 14.

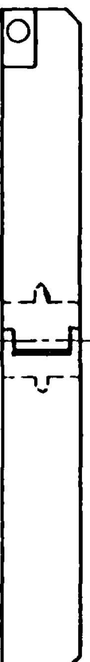

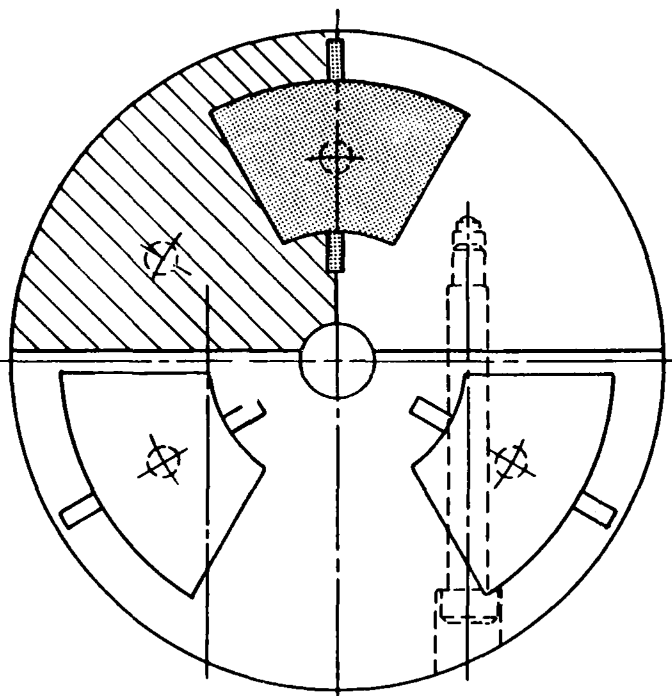

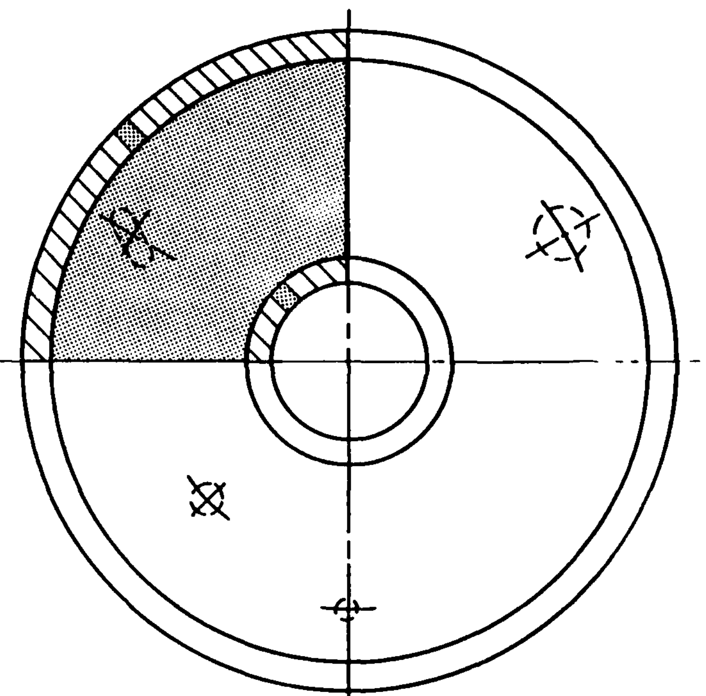

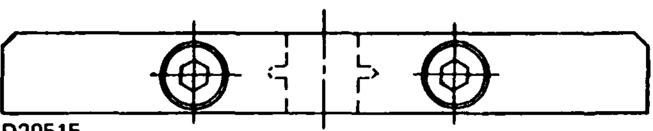

Figure 11. Capacitive film patterns.

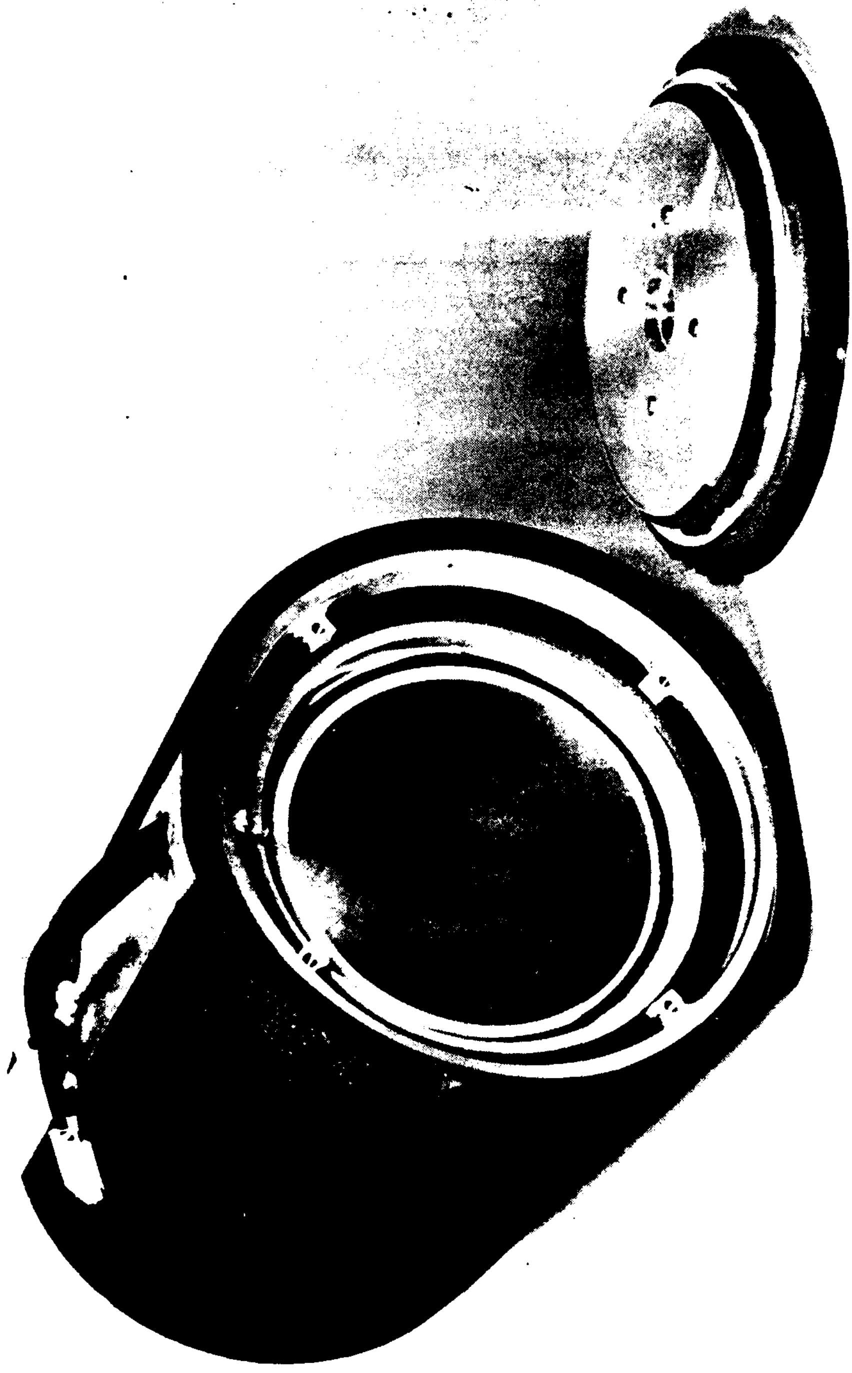

Figure 12. Oven for controlling specimen temperature.

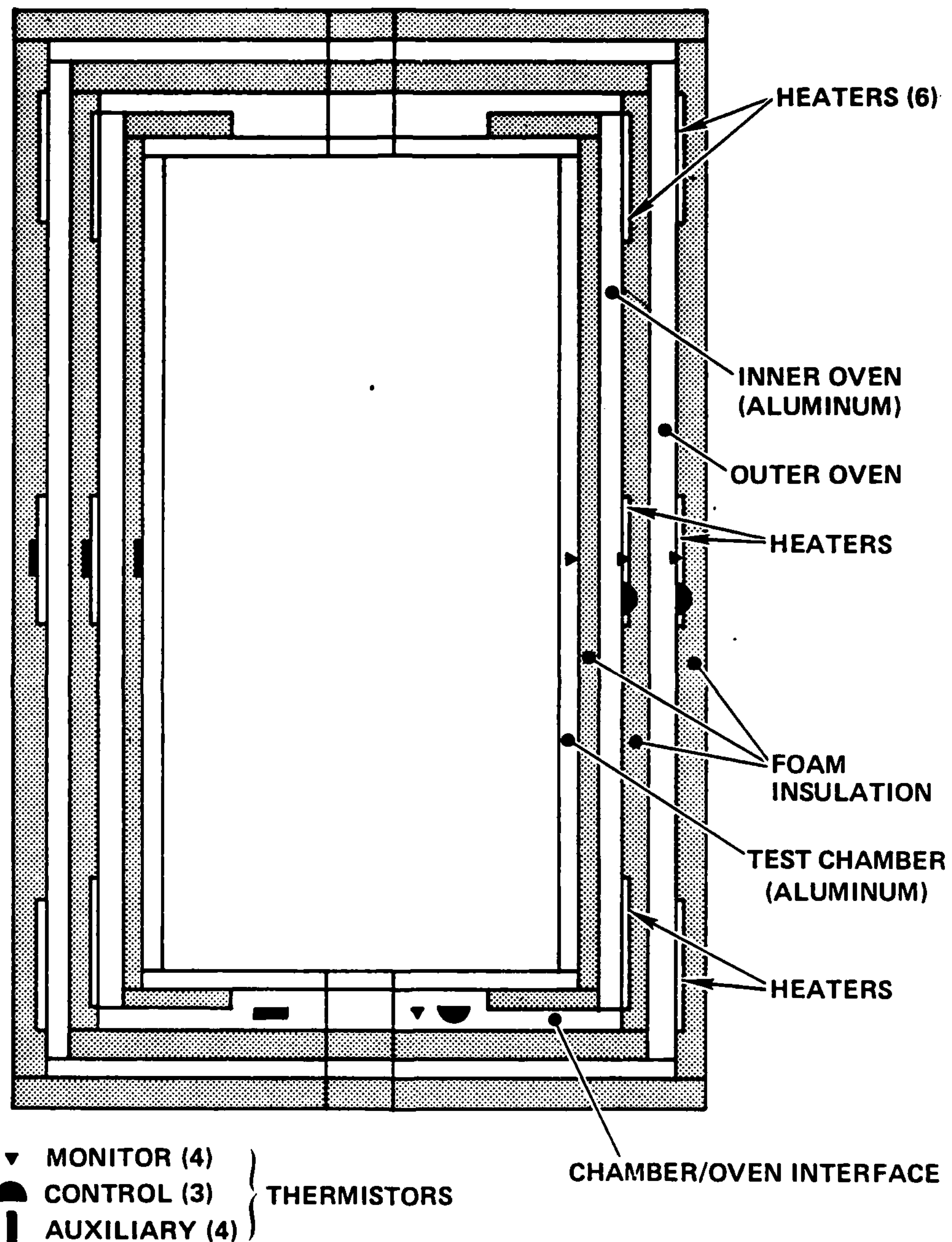

Figure 13. Micro-creep test thermal chamber.

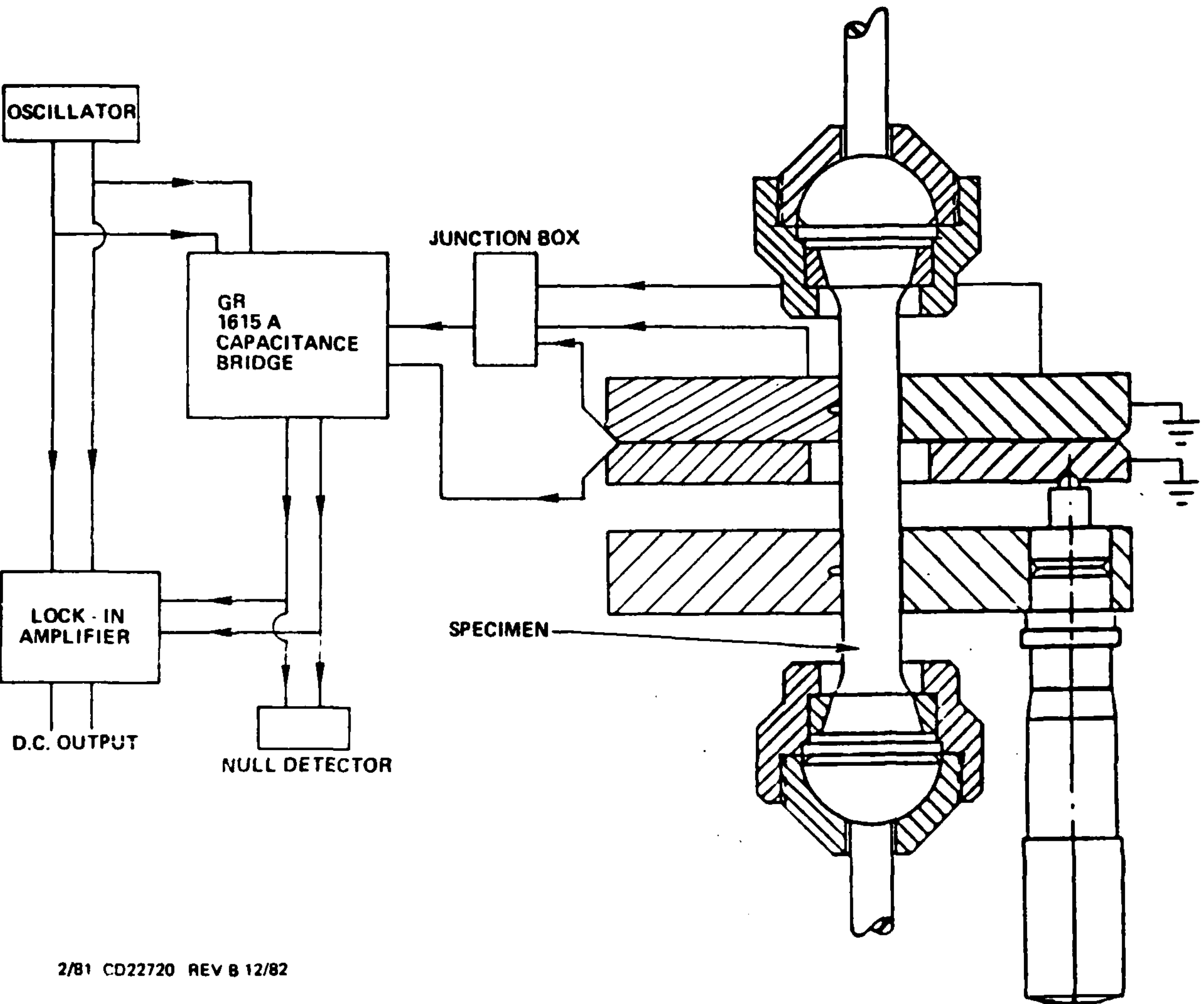

Figure 14. Schematic diagram showing capacitive signal detection of microcreep extensometer.

LIST OF REFERENCES

(1) Kumar, K., J. McCarthy, F. Petri, and J. Wollam, Materials Research for Advanced Inertial Instrumentation, Task 1: Dimensional Stability of Gyro Structural Materials, The Charles Stark Draper Laboratory, Inc., Report No. R-1433, December 1980.

(2) Polvani, R., National Bureau of Standards (NBS), Gaithersburg, Maryland (private communication).

(3) McCarthy, J., and F. Petri, Materials Research for Advanced Inertial Instrumentation, Task 1: Dimensional Stability of Gyro Structural Materials, The Charles Stark Draper Laboratory, Inc., Report No. R-1231, September 1978.

(4) McCarthy, J., and F. Petri, Materials Research for Advanced Inertial Instrumentation, Task 1: Dimensional Stability of Gyro Structural Materials, The Charles Stark Draper Laboratory, Inc., Report No. R-1388, June 1980.

(5) Kumar, K., F. Petri, and J. Wollam, Materials Research for Advanced Inertial Instrumentation, Task 1: Dimensional Stability of Gyroscope Structural Materials, The Charles Stark Draper Laboratory, Inc., Report No. R-1527, December 1981.

(6) Paine, R.M., and A.J. Stonehouse, Investigation into Effects of Microalloying and Thermal Treatment on the Properties of Beryllium, Final Report on Contract N60921-72-C-028, Brush-Wellman, Inc., Report BW-TR-549, Cleveland, Ohio, 1974.

(7) Polvani, R.S., B.W. Christ, and E.R. Fuller, Jr., "Beryllium Microdeformation Mechanisms," published in Creep and Fracture of Engineering Materials and Structure, Edited by B. Wilshire and D.R.J. Owen, Pineridge Press, Swansea, U.K., 1981.

BASIC DISTRIBUTION LIST

ORGANIZATION	COPIES
Defense Documentation Center Cameron Station Alexandria, VA 22314	12
Office of Naval Research Department of the Navy 800 N. Quincy Street Arlington, VA 22217	1
ATTN: Code 471	1
Code 102	1
Code 470	1
Commanding Officer Office of Naval Research Branch Office Building 114, Section D 666 Summer Street Boston, MA 02210	1
Commanding Officer Office of Naval Research Branch Office 536 South Clark Street Chicago, IL 60605	1
Naval Research Laboratory Washington, DC 20375	
ATTN: Code 6000	1
Code 6100	1
Code 6300	1
Code 6400	1
Code 2627	1
Naval Air Propulsion Test Center Trenton, NJ 08628 ATTN: Library	1
Naval Construction Battalion Civil Engineering Laboratory Port Hueneme, CA 93043 ATTN: Materials Division	1
Naval Electronics Laboratory San Diego, CA 92152 ATTN: Electron Materials Sciences Division	1
Naval Missile Center Materials Consultant Code 3312-1 Point Mugu, CA 92041	1
Commanding Officer Naval Surface Weapons Center White Oak Laboratory Silver Spring, MD 20910 ATTN: Library	1
David W. Taylor Naval Ship Research and Development Center Materials Department Annapolis, MD 21402	1
Naval Undersea Center San Diego, CA 92132 ATTN: Library	1
Naval Underwater System Center Newport, RI 02840 ATTN: Library	1
Naval Weapons Center China Lake, CA 93555 ATTN: Library	1

BASIC DISTRIBUTION LIST (continued)

ORGANIZATION	COPIES
Naval Air Development Center Code 302 Warminster, PA 18964 ATTN: Mr. F.S. Williams	1
Naval Air Systems Command Washington, DC 20360 ATTN: Code 52031 Code 52032	 1 1
Naval Sea System Command Washington, DC 20362 ATTN: Code 035	1
Naval Facilities Engineering Command Alexandria, VA 22331 ATTN: Code 03	1
Scientific Advisor Commandant of the Marine Corps Washington, DC 20380 ATTN: Code AX	1
Naval Ship Engineering Center Department of the Navy Washington, DC 20360 ATTN: Code 6101	1
Army Research Office P.O. Box 12211 Triangle Park, NC 27709 ATTN: Metallurgy and Ceramics Program	1
Army Materials and Mechanics Research Center Watertown, MA 02172 ATTN: Research Programs Office	1
Naval Postgraduate School Monterey, CA 93940 ATTN: Mechanical Engineering Dept.	1
NASA Headquarters Washington, DC 20546 ATTN: Code RRM	1
NASA (216) 433-4000 Lewis Research Center 21000 Brookpark Road Cleveland, OH 44135 ATTN: Library	1
National Bureau of Standards Washington, DC 20234 ATTN: Metallurgy Division Inorganic Materials Division	1
Director Applied Physics Laboratory University of Washington 1013 Northeast Fortieth Street Seattle, WA 98105	1
Defense Metals and Ceramics Information Center Battelle Memorial Institute 505 King Avenue Columbus, OH 43201	1
Metals and Ceramics Division Oak Ridge National Laboratory P.O. Box X Oak Ridge, TN 37380	1
Los Alamos Scientific Laboratory P.O. Box 1663 Los Alamos, NM 87544 ATTN: Report Librarian	1

BASIC DISTRIBUTION LIST (continued)

ORGANIZATION	COPIES	ORGANIZATION	COPIES
Air Force Office of Scientific Research Bldg. 410 Bolling Air Force Base Washington, DC 20332 ATTN: Chemical Science Directorate Electronics and Solid State Sciences Directorate		Argonne National Laboratory Metallurgy Division P.O. Box 229 Lemont, IL 60439	1
Library Building 50, Rm. 134 Lawrence Radiation Laboratory Berkeley, CA	1	Office of Naval Research Branch Office 1030 East Green Street Pasadena, CA 91106	
Brookhaven National Laboratory Technical Information Division Upton, Long Island New York 19973 ATTN: Research Library	1		

SUPPLEMENTARY DISTRIBUTION LIST

Dr. Bruce W. Christ
Division 562
National Bureau of Standards
325 S. Broadway
Boulder, CO 80303

Dr. Robert S. Polvani
Room B-120, Materials Bldg.
National Bureau of Standards
Washington, DC 20234

Dr. A.W. Ruff, Jr.
National Measurement Laboratory
National Bureau of Standards
Washington, DC 20234

Dr. Robert Hocken
Room B-104, Metrology Bldg.
National Bureau of Standards
Washington, DC 20234

Dr. Gilbert J. London
Code 2023
Naval Air Development Center
Warminster, PA 18974

Professor G.S. Ansell
Rensselaer Polytechnic Institute
Dept. of Metallurgical Engineering
Troy, NY 12181

Professor J.B. Cohen
Northwestern University
Dept. of Material Sciences
Evanston, IL 60201

Professor M. Cohen
Massachusetts Institute of Technology
Department of Metallurgy
Cambridge, MA 02139

Professor J.W. Morris, Jr.
University of California
College of Engineering
Berkeley, CA 94720

Professor O.D. Sherby
Stanford University
Materials Sciences Division
Stanford, CA 94300

Dr. E.A. Starke, Jr.
Georgia Institute of Technology
School of Chemical Engineering
Atlanta, GA 30332

Professor David Turnbull
Harvard University
Division of Engineering and
Applied Physics
Cambridge, MA 02139

Dr. D.P.H. Hasselman
Montana Energy and MHD Research
and Development Institute
P.O. Box 3809
Butte, MT 59701

Dr. L. Hench
University of Florida
Ceramics Division
Gainesville, Fl 32601

Dr. J. Ritter
University of Massachusetts
Department of Mechanical Engineering
Amherst, MA 01002

Professor G. Sines
University of California, Los Angeles
Los Angeles, CA 90024

Director
Materials Sciences
Defense Advanced Research Projects
Agency
1400 Wilson Boulevard
Arlington, VA 22209

Professor H. Conrad
University of Kentucky
Materials Department
Lexington, KY 40506

SUPPLEMENTARY DISTRIBUTION LIST (continued)

Dr. A.G. Evans
Dept. Material Sciences and Engineering
University of California
Berkeley, CA 94720

Professor H. Herman
State University of New York
Materials Sciences Division
Stoney Brook, NY 11794

Professor J.P. Hirth
Ohio State University
Metallurgical Engineering
Columbus, OH 43210

Professor R.M. Latanision
Massachusetts Institute of Technology
77 Massachusetts Avenue
Room E-19-702
Cambridge, MA 02139

Dr. Jeff Perkins
Naval Postgraduate School
Monterey, CA 93940

Dr. R.P. Wei
Lehigh University
Institute for Fracture and Solid Mechanics
Bethlehem, PA 18015

Professor H.G.F. Wilsdorf
University of Virgini
Department of Materials Science
Charlottesville, VA 29903

Mr. Robert C. Fullerton-Batten
Kawecki Berylco Industries, Inc.
P.O. Box 1462
Reading, PA 19603

Mr. Norman Pinto
Kawecki Berylco Industries, Inc.
P.O. Box 1462
Reading, PA 19603

A.G. Gross
Mechanical Metallurgy Unit
Autonetics, Inc.
Anaheim, CA

A.J. Stonehouse
The Brush Beryllium Co.
Cleveland, OH

C.W. Marschall
Columbus Laboratories
Battelle Memorial Institute
Columbus, OH

R.E. Maringer
Columbus Laboratories
Batelle Memorial Institute
Columbus, OH

J.E. Hanafee
Lawrence Livermore Laboratory
University of California
Livermore, CA 94550

Professor J. Van der Sande
Massachusetts Institute of Technology
Room 13-5025
Cambridge, Massachusetts 02139

Dr. Phil Clarkin
Metallurgy and Ceramics
Office of Naval Research
6th Floor, Room 619
800 N. Quincy Street
Arlington, VA 22217

SUPPLEMENTARY DISTRIBUTION LIST (continued)

Mr. George Keith
Kawecki Berylco Industries, Inc.
P.O. Box 1462
Reading, PA 19603

Mr. Bruce Borchardt
Room B-104, Metrology Bldg.
National Bureau of Standards
Washington, DC 20234

Dr. R.F. Karlak
Lockheed Missiles & Space Co.
3251 Hanover Street
Palo Alto, California 94304

Mr. Tom Charlton
Room B-104, Metrology Bldg.
National Bureau of Standards
Washington, DC 20234

Dr. James Marder
Brush-Wellman Co.
17876 Saint Claire Avenue
Cleveland, Ohio 44110

Dr. J. Smugeresky
Sandia National Laboratories
Livermore, California 94550

3-83

DTIC